

**Understanding and forecasting the solar cycle variability
using the polar magnetic field**



**Thesis submitted in fulfilment
for the Award of
PhD
in
PHYSICS**

*by
Pawan Kumar*

DEPARTMENT OF PHYSICS
**INDIAN INSTITUTE OF TECHNOLOGY
BANARAS HINDU UNIVERSITY
VARANASI 221005**

ROLL NUMBER
18171507

YEAR OF SUBMISSION
2023

Certificate

It is certified that the work contained in the thesis titled **Understanding and forecasting the solar cycle variability using the polar magnetic field** by **Mr. Pawan Kumar**, Roll Number **18171507**, has been carried out under my supervision, and this work has not been submitted elsewhere for any degree,

Signature: *Bidyabinay Kar*

Assistant Professor
Department of Physics
Indian Institute of Technology
(Banaras Hindu University)
Varanasi-221005

Supervisor
(Affiliation)

Declaration

I, **Mr. Pawan Kumar**, certify that the work embodied in this thesis is my own bonafide work and carried out by me under the supervision of **Dr. Bidya Binay Karak** from 2019 to 2023 at the **Department of Physics, Indian Institute of Technology (BHU), Varanasi**. The matter embodied in this thesis has not been submitted for the award of any other degree/diploma. I declare that I have faithfully acknowledged and given credits to the research workers whenever and wherever their works have been cited in my work in this thesis. I further declare that I have not wilfully copied any others' work, paragraphs, text, data, results, etc., reported in journals, books, magazines, reports dissertations, theses, etc., or available at websites and have not included them in this thesis and have not cited as my own work.

Date: October 10, 2023

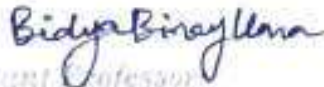
Signature 

Place: Varanasi

IIT (BHU), Varanasi


Certificate by the Supervisor

It is certified that the above statement made by the student is correct to the best of my knowledge.

Signature: 

Assistant Professor
Department of Physics
Indian Institute of Technology
Banarasi Hindu University,
Varanasi-221005

Supervisor
(Affiliation)


Signature of the Head of the Department
Head
(Physics)
Department of Physics
Indian Institute of Technology
(IIT) (BHU)
Varanasi-221005

Copyright Transfer Certificate

Title of the Thesis: Understanding and forecasting the solar cycle variability using the polar magnetic field

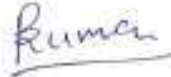
Name of the Student: Mr. Pawan Kumar

Copyright Transfer

The undersigned hereby assigns to the Institute of Technology (Banaras Hindu University) Varanasi all rights under copyright that may exist in and for the above thesis submitted for the award of the **PhD in Physics**.

Date: October 10, 2023

Signature



Place: Varanasi

IIT (BHU), Varanasi

Note: However, the author may reproduce or authorize others to reproduce material extracted verbatim from the thesis or derivative of the thesis for the author's personal use provided that the source and the Institute's copyright notice are indicated.

*In loving memory of
my Father*

Acknowledgements

First and foremost, I offer my heartfelt praises and thanks to *Parmatma* (God), the Almighty, for His showers of blessings throughout my research work to complete this research journey successfully.

I am sure that these short words cannot express my gratitude to my mentor Dr. Bidya Binay Karak, for his unwavering assistance, encouragement, and invaluable guidance. He has always been more than a thesis supervisor. Even in the face of my own limitations and the slow pace of my research progress, he has remained exceptionally cooperative and supportive. This research work would not have been achievable without his expert guidance and steadfast support. I would also like to thank my RPEC committee members for their invaluable patience and feedback.

I am privileged to thank my collaborators, Prof. Kristof Petrovay, Dr. Melinda Nagy, and Dr. Alexandre Lemerle. Through these collaborations, I have had the opportunity to learn from and engage with diverse research approaches in solar physics. I am grateful for the synergy and cooperation that we shared throughout our work, which enriched the quality and outcomes of our efforts.

I also acknowledge my lab members. I am heartily grateful to Vindya, who provided me the kind of unconditional support throughout my Ph.D. journey that means a lot to me, and I will forever be in debt to her. Vindya, Akash, and Anu's unconditional support and collaboration have been instrumental in successfully completing my Ph.D. Their dedication, expertise, and willingness to share knowledge have enriched my academic journey and contributed significantly to the quality of this work. I consider myself fortunate to have worked alongside such a talented and supportive group of individuals. There will be an unforgettable memory of having fun, parties, and roaming different places on this journey with you.

I extend my heartfelt gratitude to the administrative staff, library personnel, and the Param Shivay computational support team for their invaluable assistance and seamless facilitation of my research endeavors. Their dedication and efficiency have a lot to contribute to the success of my work. I would also like to sincerely thank the Head of the Physics Department (HOD) and all the esteemed faculty members for their guidance and continuous encouragement throughout my academic journey.

I am grateful and would like to extend my heartiest appreciation to my dear friends and batchmates Ravi, Avinash, Amit, and Sanjeet for their unwavering support and companionship during this challenging and rewarding journey of pursuing a Ph.D. Their friendship has been a constant source of motivation and solace, providing a much-needed respite from the rigors of academic life. I would also like to acknowledge my juniors Devendra, Anshul, Sanjeev, Anish, and Sachin for spending hours engaging in gossip and discussions for fun. Your presence in my life has made this journey all the more meaningful and memorable.

This journey could not have been possible without the constant support of my *Baba*, *Maa*, and my siblings. Your sacrifices, encouragement, and belief in my abilities have been my guiding light. Your unconditional love and support made it possible for me to complete this challenging journey. In addition, the kind of endless support I met from Sandeep, Uday, Tanmay, and Sadhana, I can't express in words. These have been the wheel of my life. Furthermore, it has been a blessing to have lovely young kids, Golu, Bholu, and my sweet Guddan, around me, and I am grateful to them for all the fun times we had together. Your innocent curiosity and boundless love have served me the new energy on this journey.

Data Usage

Throughout the various studies presented in this thesis, I have utilized telescopic and derived data from several ground and space-based facilities. I duly acknowledge the usage of this data. Furthermore, I also want to thank the members and associates of these facilities for their invaluable contributions in providing this data.

Wilcox Solar Observatory (WSO) has been taking the Sun's polar field data since 1976 and is located in the foothills just south of the Stanford University campus. NASA Heliophysics, the NSF, and the Office of Naval Research have supported it. The other data supply courtesy of the SOHO/MDI and SDO/HMI.

Abstract

The Sun's magnetic field exhibits a wide range of variabilities, which can be broadly classified into long-term and short-term. The cause of this magnetic field is believed to be the dynamo process, which operates in the Sun's convection zone. The large-scale magnetic field is responsible for shaping the overall solar activity, including the 11-year solar cycle and the formation of the Sun's polar field. This field exhibits extreme variability and drives space weather, leading to highly energetic events that can have direct or indirect adverse and hazardous effects on Earth's atmosphere and human society in various ways. Therefore, understanding and prediction of the irregular variability of solar magnetic field is essential.

With a renewed focus on researching "*solar magnetic field variability and forecasting*", we have developed and implemented several new automatic techniques and models for extensive data analysis and findings in this thesis. This approach enhances overall consistency and effectively eliminates the potential for human error, which has been common practice in the past. These new techniques and models are used to study the irregularities in the polar field and the solar cycle due to observed fluctuations in Bipolar Magnetic Region (BMR) properties, such as fluctuations in the BMR tilt, flux, emergence latitude, and the time delay between successive BMR emergence. Besides this, we forecast the strength of Solar Cycle 25 using the polar field and the Waldmeier effect. We have used observed data of the polar field (1974–2022) from Wilcox Solar Observatory (WSO), Polar faculae counts (1907–2011), Pulkovo observatory $A(t)$ index (1915–1999), Dipole moment (1976–2017), sunspot number SSN (1749–2022), and sunspot area SSA (1874–2022) along with 2D and 3D dynamo models. We have also explored how the memory of the polar field and the occurrence of grand minimum-like events change with the dynamo super-criticality in Babcock-Leighton-type dynamo models.

The extensive analysis of irregular BMR properties reveals that their cumulative impact sufficiently generates irregularities in the polar field and the solar cycle consistent with observed patterns. Additionally, this analysis indicates that the maximum variability in the polar field and the solar cycle is produced due to scatter in BMR tilt around Joy's law. It is worth noting that many researchers have developed different prediction methods for future solar cycle variability using mathematical and statistical methods. However, most of the time, these methods give diverging results from observations.

For forecasting the irregular solar cycle strength, we utilized the polar precursor method, a widely accepted physics-based approach. In this process, we computed the Pearson correlation coefficient between the previous cycle polar field and peak sunspot number as a function of time. Using this, we predicted the upcoming solar cycle strength after four years of the polar field reversal, typically 2 to 3 years before the solar minimum and about seven years before the predicted maximum. Different utilized dynamo models in this work produce similar results and thus increase the reliability of this result. However, researchers conventionally made the prediction of the next cycle using the polar field as a precursor at cycle minimum. Our prediction for Cycle 25's amplitude, based on the WSO polar field, suggests it will be stronger than Cycle 24 and only deviates from the conventional prediction at the cycle minimum by $3.1 \pm 14.7\%$.

We further show the strong linear correlation between the polar field rise rate of the preceding cycle and the next solar cycle amplitude. This correlation enables us to predict the solar cycle strength 9 years earlier than its maximum. Furthermore, the polar field rise rate of the preceding cycle and the solar cycle rise rate show a strong linear correlation, showing the physical connection between the polar field buildup and the well-known Waldmeier effect.

This forecasting ability comes from the memory of the Sun's polar field and depends on the dynamo super-criticality. An extensive analysis of different Babcock-Leighton-type

dynamo reveals that when the dynamo operates near the critical region, the polar field can decide multiple cycle strengths (at least three). Furthermore, when the dynamo operates in the supercritical region, the polar field can decide only the next cycle strength. This change in the memory of the polar field is independent of the importance of various turbulent transport processes in the models. We also find that near the critical region, the dynamo produces frequent extended episodes of weaker activity i.e., solar grand minima. The frequency of grand minima decreases with the increase of dynamo super-criticality.

Thus, the Sun's polar field, generated through the Babcock-Leighton process, is used to study the variability and forecasting of the solar cycle. The variability and prediction memory observed in the polar field are contingent upon the inherent randomness and nonlinearity in the BL process, stemming from the irregularities in BMR properties on the solar surface.

Table of contents

List of figures	xix
List of tables	xxviii
Nomenclature	xxviii
1 Introduction	1
1.1 Solar Magnetism and Cycle	3
1.2 Proxies of Solar Magnetism	10
1.3 Prediction of Solar Activity and its Necessity	12
1.4 Origin of Solar Magnetism	14
1.4.1 Basics of Magnetohydrodynamics	15
1.4.2 Magnetoconvection	17
1.4.3 Essentials of Solar Dynamo	18
1.4.4 Babcock–Leighton Dynamo Model for Solar Cycle	31
2 Variability in Sun’s magnetic field due to irregular properties of BMRs	35
2.1 Introduction	36
2.2 Model	39
2.2.1 STABLE model	41
2.2.2 Deposition of synthetic BMRs in STABLE	43

2.3	Results and Discussion	44
2.3.1	Variation in the polar field	44
2.3.2	Variation in the solar cycle	50
2.4	Conclusions	54
3	Solar cycle prediction using polar precursor method with different predictors	55
3.1	Introduction	56
3.2	Observational data analysis	59
3.2.1	Data	59
3.2.2	Solar cycle landmarks	60
3.2.3	Correlations in the observed data	62
3.3	The polar precursor in solar dynamo models	65
3.3.1	Surya dynamo model	67
3.3.2	STABLE dynamo model	70
3.3.3	$2 \times 2D$ dynamo model	71
3.4	Conclusions	74
4	Physical Link of Polar Field Buildup With Waldmeier Effect and Solar Cycle Prediction	78
4.1	Introduction	79
4.2	Data and Methods	81
4.3	Results and Discussion	81
4.3.1	WE2 and the prediction of Cycle 25	81
4.3.2	Connecting WE2 with the previous cycle polar field	84
4.3.3	Correlation with the rise rate of the polar field and the prediction of Cycle 25	86
4.4	Conclusions	88

5	Dynamo supercriticality and memory of the polar field	91
5.1	Introduction	92
5.2	Models	94
5.2.1	Flux Transport Dynamos	95
5.2.2	Time Delay Dynamo	97
5.3	Results from Flux Transport Dynamo Models	97
5.3.1	Identifying critical dynamo parameters	99
5.3.2	Identifying the correlation of polar field	100
5.4	Results from Time Delay Dynamo Model	110
5.5	Comments on the conclusion of Yeates et al. (2008)	111
5.6	Conclusions and Discussions	112
6	Conclusions and future outlook	115
	References	119

List of figures

1.1	Image of the group sunspots and surrounding granules on the solar surface for the active region(AR) 10030. The image was taken on 15 July 2002 by Swedish 1-m solar Telescope. The image has been colored yellow for aesthetic reasons. (<i>Image courtesy: Royal Swedish Academy of Sciences</i>).	4
1.2	Vertical flux density map, calculated from the MDI line-of-sight magnetogram recorded on 2002 April 26. The IDL program has identified 10 bipolar magnetic regions and enclosed them in rectangular boxes. The gray-scale cuts are set at +2.5 kG (blue) and -2.5 kG (red). (<i>Image courtesy: Sreedevi et al. (2023)</i>).	5
1.3	Time-latitude distribution of the sunspots (butterfly diagram), showing the emergences below about $\pm 40^\circ$ latitudes. Note that in every cycle, the latitudes of sunspots drift toward the equator as the cycle progresses. (<i>Source: https://vizier.cfa.harvard.edu/</i>).	6

- 1.4 Time series plot of the polar field of the Sun for northern (black) and southern (blue) hemispheres. We have used Gaussian smoothing filter (Hathaway et al., 2002a) with FWHM = 6 months for smoothing the data. This field is computed by averaging the radial field (derived from the measured line-of-sight component) from 55° to the poles. To remove the yearly geometric projection effect, a 20 nHz low pass filter has been used during the recording of the data. (*Source: Wilcox Solar Observatory, <http://wso.stanford.edu/Polar.html>*). 7
- 1.5 Time-latitude distribution of the longitudinal average radial field on the solar surface. This image illustrates the polarity reversals, the generation of the poloidal field from the decay of active regions at low latitudes, and the drift of the field towards the polar region. Black contours represent the locations of high activity regions (sunspot band). Green and yellow points represent the non-Joy and anti-Hale active regions (ARs). (*Image courtesy: Mordvinov et al. (2022)*). 8
- 1.6 Temporal variation of monthly mean sunspot number (ISN V2.0) smoothed using a Gaussian filter of FWHM = 7 months (red dashed curve), available since 1749, and the yearly mean group sunspot number (black curve) available during 1610–2015. Note that the group sunspot number is scaled by a factor of 18 to bring it to the scale of the sunspot number. The blue curve is the Gleissberg cycle, with a time period of 98 years. Cycle numbers for which the Gnevyshev–Ohl rule (Even–Odd rule) is obeyed are shown by indicating the number on the odd cycles. (*Source: WDC–SILSO, Royal Observatory of Belgium, Brussels, <https://www.sidc.be/SILSO/datafiles>, Image courtesy: Karak (2023)*). 9

-
- 1.7 Time series of different proxies of solar magnetism. (a) Sunspot area. (b) Sunspot number reconstructed from radioisotopes. (c) Hemispheric polar faculae count. (d) $A(t)$ index. (e) Hemispheric Polar Network Index (PNI). 11
- 1.8 Temporal variation of monthly mean sunspot number (ISN V2.0) and monthly mean solar flare index. Note that the flare index is scaled by a factor of 10 to bring it to the scale of the sunspot number. (*Source: WDC–SILSO, Royal Observatory of Belgium, Brussels, <https://www.sidc.be/SILSO/datafiles>, and Kandilli Observatory, Istanbul, Turkey, <https://www.ngdc.noaa.gov/stp/space-weather/solar-data/solar-features/solar-flares/index/>*). 14
- 1.9 The sketch of the magnetic buoyancy of a flux tube. (a) A nearly horizontal flux tube in the convection zone. (b) The flux tube after its upper part has risen through the solar surface due to magnetic buoyancy. The sketch is inspired by Choudhuri (1998). 23
- 1.10 (a) Meridional circulation streamlines used in the dynamo model. The dashed lines show the tachocline at the base of the convection zone (b) Variation of the latitudinal component of the meridional circulation at 45° latitude. 24
- 1.11 Diffusivity profile for the solar dynamo. Blue and black curves show the variation of toroidal diffusivity and poloidal diffusivity in the 2D *Surya* dynamo model; however, the dark red curve shows the turbulent diffusivity in the 3D dynamo model with solar radius. 26
- 1.12 The sketch of the generation of the toroidal field from the poloidal field in the solar convection zone (SCZ) due to differential rotation, i.e., Ω effect. (a) Initial poloidal field line. (b) Field line after stretches due to differential rotation in the Sun, (*Image courtesy: Choudhuri (1998)*). 27

1.13	Differential rotation profile from the model.	28
1.14	The sketch of the different stages of the dynamo process. (a) Initial poloidal field line stretches due to Ω effect. (b) Twisting in the toroidal field lines due to helical turbulence. (c) Generation of the poloidal field from turbulent α effect, (<i>Image courtesy: (Choudhuri, 1998)</i>).	29
1.15	Babcock–Leighton mechanism demonstration (for three years) through decay and dispersal of two BMRs deposited at 25° latitude symmetrically in both hemispheres. BMRs tilt assigned by Joy’s law and weak poloidal field deposited at the poles after three years are shown, (<i>Image courtesy: (Karak, 2023)</i>).	30
1.16	Cartoon representation of the Babcock–Leighton dynamo loop.	33
1.17	The details of the Babcock–Leighton dynamo model in a meridional cut of the solar convection zone (<i>Image courtesy: (Cameron & Schüssler, 2023)</i>).	33
2.1	Distributions of (a) the time delay between two successive BMR emergences and (b) flux content of 8800 BMRs obtained from MDI and HMI magnetograms during 1996–2020. Quantities are obtained by tracking each BMR throughout its lifetime or disk passage and taking the average values during the time when the flux is above 70% of its maximum (Sreedevi et al., 2023). The solid lines are the log-normal distributions that approximately fit the data and they will be used in our calculations and was also used in Karak & Miesch (2017).	39
2.2	The results produced from STABLE dynamo model. (a) Time evolution of the axial dipole moment (D) of a BMR deposited at different latitudes with constant flux (F) of 10^{22} Mx and tilt (α) of 80° . (b) The values of the saturated (final) dipole moment vs the latitude of single BMR. The solid curve is the Gaussian fit of the form $\exp(-\lambda^2/110)$	40

2.3	The plot shows the effect of time delays in successive BMR eruptions on the polar field. The black curve shows a reference polar field in the plot (see inset for the zoomed-in view).	45
2.4	Format of each panel is the same as Figure 2.3, but shows the evolution of the polar field from simulations with (a) variation in the BMRs flux, (b) variation in BMRs latitude, (c) scatter in BMR tilt, and (d) combined fluctuations.	46
2.5	Temporal variations of (a) the monthly numbers of BMRs (red/black: north/south) and (b) the azimuthal-averaged surface radial field from the simulations in which the time delay in BMR eruption is random.	48
2.6	Same as Figure 2.5 but from the simulation in which BMR flux is irregular.	49
2.7	Same as Figure 2.5 but from the simulation in which the tilt has a scatter around Joy's law.	50
2.8	Same as Figure 2.5 but from simulations including all fluctuations (i.e., time delay, flux, latitude, and tilt) and the time delays are magnetic field independent.	51
2.9	Same as Figure 2.8 but with magnetic field-dependent time delay.	52
3.1	Scatter plot of the peak value of the polar field (or its proxy) vs the peak sunspot area in the following cycle for (a) WSO polar field (Cycles 21 to 24), (b) Dipole moment (Cycles 21 to 24) (c) MWO polar faculae (Cycles 14 to 23), and (d) Pulkovo Observatory $A(t)$ index (Cycles 15 to 22). Sunspot areas in (a) and (c) are hemispheric peak values, while in (b) and (d) the peak value of the hemispheric average.	61

- 3.2 Pearson's correlation coefficient = $\text{Corr}[T(t_{\max}), P(t)]$ between the peak sunspot area T at the maximum of the next cycle and polar field measures $P(t)$ as a function of time (a) measured backward from the cycle maximum: $t = t_{\max} - \tau$, (b) measured forward from the reversal of P : $t_{\text{rev}} + \tau$. Vertical lines indicate the average positions of other cycle landmarks in the given plot, with the same color coding as the associated curves. (a) Black dots: cycle minimum $T_{\text{SSA},\text{min},i}$, dashed lines: time shift from the time of the maximum of $|P|$ to next cycle maximum $T_{\text{p,max},i-1} \rightarrow T_{\text{SSA},\text{max},i}$. (b) Dashed lines: time shift from reversal of P to cycle minimum $T_{\text{p,rev},i-1} \rightarrow T_{\text{SSA},\text{min},i}$ 63
- 3.3 Time series of some predictors P (blue and black) and predicted activity indicators T (red). (a) Observations; (b) Surya 2DR1 model; (c) STABLE 3DR1 model; (d) $2 \times 2\text{D-R1}$ model. Some example intervals used for the determination of rise and decay rates (see Appendix) of P are marked. Rise and decay rates in cycle n are defined as $(P2(n) - P1(n))/(t2(n) - t1(n))$ and $(P4(n) - P3(n))/(t4(n) - t3(n))$, respectively. 65
- 3.4 Same as Fig. 3.2, for different parameterizations of the Surya dynamo model. PF: polar cap flux; DM: global dipole moment. Vertical lines mark the mean positions of cycle landmarks with the same colour coding as the associated curves. (a) Black dots: cycle minimum $T_{\text{SSN},\text{min},i}$, dashed lines: time shift from the time of the maximum of $|P|$ to next cycle maximum $T_{\text{p,max},i-1} \rightarrow T_{\text{SSN},\text{max},i}$. (b) Dashed and dot dashed lines show the time shift from reversal of P to cycle minimum $T_{\text{p,rev},i-1} \rightarrow T_{\text{SSN},\text{min},i}$, respectively for dipole moment and polar field. 68
- 3.5 Same as Fig. 3.4, for different parameterizations of the STABLE dynamo model. 70

- 3.6 Same as Fig. 3.4, for the $2 \times 2D$ dynamo model. 73
- 4.1 Scatter plots between the rise rates and the amplitudes of the cycles for SSN (a) and SSA (b). Lines are the linear regressions: $y = mx + c$, where $m = 2.001 \pm 0.308$ and $c = 77.305 \pm 16.545$ for SSN and $m = 2.423 \pm 0.114$ and $c = 596.789 \pm 62.028$ for SSA. 83
- 4.2 Comparison of our prediction with observations. Temporal variation of the observed SSN is shown by the blue curve. The predicted amplitudes are shown by black squares and their errors by vertical lines. The time of the peak of the predicted Cycle 25 is shown by the vertical dotted line with the error by a horizontal arrow. The prediction for Cycle 25 using *the rise rate* of the previous cycle's polar field is shown by a (dark red) filled circle. 83
- 4.3 Scatter plots between the polar field at solar cycle minimum and the rise rate of next cycle. (a) Open circles and red crosses represent the rise rates calculated from SSN and SSA, respectively. (b) Same as (a) but from a Babcock–Leighton type dynamo model. 84
- 4.4 (a) Scatter plot between rise rate of observed polar field and the amplitude of the next cycle SSN. Regression lines: $y = mx + c$, where $m = 3.677 \pm 0.876$ and $c = 29.093 \pm 13.517$ for the northern (asterisks) and $m = 3.689 \pm 0.912$ and $c = 33.405 \pm 15.311$ for southern hemispheres (filled circles). (b) Same as (a) but from the dynamo model. (c) scatter plot between rise rate of the observed polar field and the rise rate of next cycle SSN. Asterisks and filled circles represents northern and southern hemispheres respectively. (d) Same as (c) but from the dynamo model. 89

- 5.1 (a): Variation of the toroidal flux ϕ_{tor} with the strength of the Babcock-Leighton α_0 from Models I (solid) and II (dashed). The critical α_0 , α_0^{crit} for Models I and II are 6.2 m s^{-1} and 10 m s^{-1} . (b): Same as (a) but obtained from Model III and IV (shown in inset); note in these models, $\alpha_0^{\text{crit}} = 0.38$ and 0.05 m s^{-1} 98
- 5.2 Same as Figure 5.1 (c): For Model V (no meridional circulation); $\alpha_0^{\text{crit}} = 0.8 \text{ m s}^{-1}$. (d) For Model VI (η_0 is varied; note $\eta_0^{\text{crit}} = 0.05 \times 10^{12} \text{ cm}^2 \text{ s}^{-1}$). 98
- 5.3 Scatter plots between the peaks of the surface polar flux of cycle n , $\phi_r(n)$ with that of the low-latitude toroidal flux at the base of CZ, ϕ_{tor} of cycle (a) n , (b) $n + 1$, (c) $n + 2$, and (d) $n + 3$ from Models I (blue/circles) and II (red/asterisks). Top four and bottom four panels are obtained from runs at weakly supercritical ($\hat{\alpha}_0 = 2$) and highly supercritical ($\hat{\alpha}_0 = 4$) dynamos, respectively. For Model I data, a factor of two is multiplied to $\phi_r(n)$ in top four panels and in the bottom four panels 2.8 and 1.04 are multiplied to $\phi_r(n)$ and $\phi_{\text{tor}}(n)$, respectively for comparison. 102
- 5.4 Time series of polar flux from Model I for (a) $\hat{\alpha} = 2$ (weakly supercritical), (b) $\hat{\alpha} = 2.5$, and (c) $\hat{\alpha} = 4$ (highly supercritical). Red color highlights the weaker activity episodes. 103
- 5.5 The format is same as Figure 5.3 but obtained from Model V at $\alpha_0 = 0.4 \text{ m s}^{-1}$. Top four and bottom four panels are obtained from a weakly supercritical ($\hat{\eta}_0 = 1$) and highly supercritical dynamos ($\hat{\eta}_0 = 4$), respectively. 104

-
- 5.6 Results from the time delay dynamo model: Variations of the correlation coefficients of the peak poloidal fields of cycle n with the peak toroidal fields of cycle n (black line), $n + 1$ (red), $n + 2$ (blue), and $n + 3$ (green) with 30% fluctuations. In the left panel, τ_d is fixed at 15 and α_0 is increased, while in right panel, α_0 is fixed at 0.29 and τ_d is increased. 108
- 5.7 Same as Figure 5.6(a) but at higher α fluctuations; dotted and dashed for 45% and 100% fluctuations, respectively. 109
- 5.8 Top and bottom: Time series of surface polar flux from Models I and II at $\alpha_0 = 30 \text{ m s}^{-1}$ (or $\hat{\alpha} = 4.8$ and 3) which respectively correspond to the diffusion- and advection-dominated models of Yeates et al. (2008). . . . 112

List of tables

2.1	Variability σ and the maximum possible percentage variability produced in the polar field due to different individual fluctuation parameters of the BMRs relative to the combined fluctuations (Figure 2.4(d); $\sigma = 2.39$ G).	45
3.1	Relative time shifts (in years) between different solar cycle landmarks: observations and models. The number of cycles used in the analysis are 270, 200, and 260, respectively for models 2DR1, 3DR1, and $2 \times 2D$ -R1. The symbol '— —' indicates that the values are the same as given in the previous column.	58
4.1	Predictions of the solar cycle <i>amplitudes</i> using the rise rates of SSN and SSA (in μ Hem) for the last few known cycles and the ongoing Cycle 25.	83
4.2	Comparison of our predictions for Solar Cycle 25 (P1: using the rise rate of the SSN, P2: using the rise rate of the previous cycle's polar field) with predictions by other groups who used observed polar precursor.	88
5.1	Correlation coefficients between ϕ_r (n) and ϕ_{tor} of different cycles for simulations at different values of $\hat{\alpha}_0$ and $\hat{\eta}_0$	101
5.2	The mean cycle period T_{av} of the simulations presented in Table 5.1. . . .	101
5.3	The same as Table 1 but only for Model IV and at increased fluctuation levels.	103